Norwegian Meteorological Institute
met.no

met.no report

no. 6/2009
Air Pollution & Remote Sensing

Further development AOD observation operator and testing with MODIS data

AeroKval project report

Svetlana Tsyro

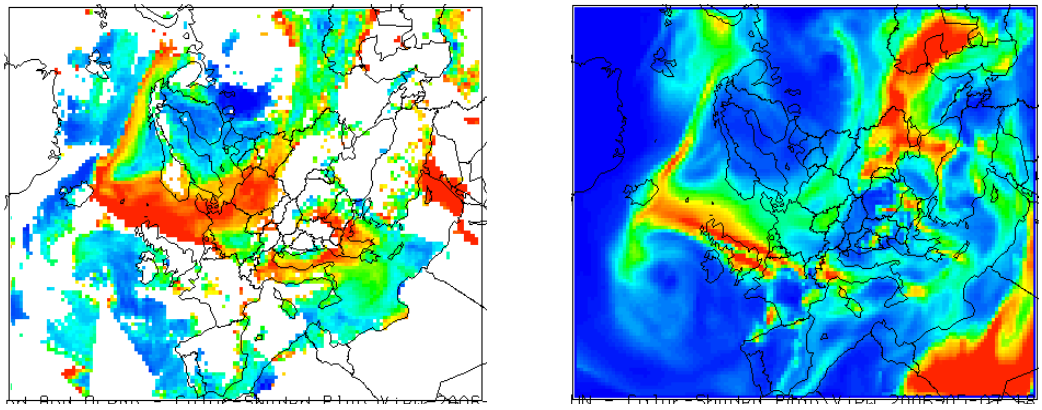

Agricultural fire event, 7 May 2006
AOD at 0.55 μm: MODIS retrieval (left) and the EMEP model (right)

Norwegian Meteorological Institute
met.no

report

Title	Date
Further development of AOD observation operator and testing with MODIS data	20 April 2009
Section Air Pollution and Remote Sensing, R&D Department.	**Report no.** 6
Author(s) Svetlana Tsyro	**Classification** ◯ Free ◯ Restricted
	ISSN 1503-8025
	e-ISSN
Client(s) Norwegian Space Centre	**Client's reference**

Abstract. In this report, the main results and findings obtained during 2008 within the AeroKval project (WP 1) are presented. The AOD observation operator, which was developed during the first year of the project, has been further developed and tested both with a box-model and within the EMEP aerosol model. The recent revisions of the AOD observation operator have appreciably improved the agreement between model calculations and MODIS AOD retrievals. On average, model calculated AOD is between 33 and 45% lower than MODIS retrievals and the spatial correlation is between 0.24 and 0.36 in different seasons in 2004 and 2006. For a number of grid cells containing EMEP measurement sites the temporal correlation between calculated and MODIS AOD is mostly between 0.4 and 0.7 and often better than the correlation between calculated and measured $PM_{2.5}$ (or PM_{10}).

Further testing of the AOD observation operator within the EMEP aerosol model has been performed for a pollution event due to large agricultural fires in western Russia and Eastern Europe in spring 2006. In general, the model manages quite well to reproduce the main features of AOD fields and the propagation of enhanced AOD associated with fires as observed by MODIS. Additionally, model calculated AOD has been compared with AOD measurements from sun photometers and with MODIS AOD retrievals for five sites affected by the fire emissions. Calculated AOD correlates reasonably well with MODIS and sun photometer AOD, while the model systematically underestimated measured AOD.

Keywords
Satellite aerosol observations, MODIS aerosol products, AOD, EMEP chemical transport model.

Disiplinary signature	Responsible signature
_____	_____

Postal address P.O.Box 43, Blindern NO-0313 OSLO Norway
Office Niels Henrik Abelsvei 40
Telephone +47 22 96 30 00
Telefax +47 22 96 30 50
e-mail: met@met.no **Internet:** met.no
Bank account 7694 05 00628
Swift code DNBANOKK

Postal address
P.O.Box 43, Blindern
NO-0313 OSLO
Norway

Office
Niels Henrik Abelsvei 40

Telephone
+47 22 96 30 00

Telefax
+47 22 96 30 50

e-mail: met@met.no
Internet: met.no

Bank account
7694 05 00628

Swift code
DNBANOKK

1. Introduction

Making use of satellite observations is a relatively recent practise in assessing the chemical state of atmosphere. Until the last decade, ground-based measurements of pollutant surface concentrations were mostly employed for monitoring air pollution and for model validations. Last decade, satellite measurements of the atmospheric load of gaseous and aerosol species has increasingly been taken in use for evaluation of chemical transport models and for data assimilation in chemical weather forecasting.

Monitoring of air pollution from the satellites has several significant advantages compared to ground-based in-situ surface measurements and remote sensing. One of the main merits of satellite measurements is their geographical coverage. Most of the polar-orbiting satellites, including Aqua and Terra carrying MODIS instruments on board, are able to observe almost the entire Earth surface everyday. Moreover, the satellite surveillance is a powerful instrument in detecting pollution episodes, caused for example by volcano eruptions, desert storms or wildfires. Thus, satellites provide very useful data for evaluation of the model ability to reproduce pollution transport, which is particularly valuable in the regions with a lack of surface monitoring. Finally, satellite measurements, available in the near-real time regime, can be assimilated within model forecasts of the chemical weather in order to improve the forecast skill.

In the first year of the AeroKval project, an observation operator for AOD (aerosol optical depth) was developed and implemented in the EMEP chemical transport model. The description of the AOD observation operator and first results from model calculations of AOD for the years 2003 and 2004 were presented in our previous report to NRS (met.no Report 11/2007, Tsyro et al., 2007). Comparison of model calculated AOD with AOD retrievals from MODIS data aboard the Aqua and Terra satellites showed a fair agreement for different seasons in 2003 and 2004. The model showed a tendency to calculate lower AOD compared to MODIS data. The spatial correlation between model calculated and MODIS daily AOD was rather poor, which was thought to be partly due to generic inconsistencies between modelled AOD and MODIS retrievals of AOD, as discussed in Tsyro et al. (2007). On the other hand, the temporal correlation between calculated and MODIS AOD was fairly good.

Following the work initiated within AeroKval-2007 towards the development of an operational system of air quality forecast, in which assimilation of satellite data is an essential part, AeroKval-2008 project has focused on three work packages:

1. Further development of an observation operator for MODIS data.
2. Characterisation of NO2 data from GOME versus model results.
3. Methods for 1D-VAR data assimilation of NO2 .

This report describes the results of work package 1, while the results of work packages 2 and 3 are described in a separate report.

During the reporting period of the year 2008, the work have been carried out on further development and testing of the AOD observation operator with a box-model and within the EMEP model. New model calculations of have been performed for the year of 2006. Model AOD results have been compared with MODIS data. Focusing on the large fire event in spring 2006, we evaluated the model results with both MODIS data and AOD measurements from sun-photometers. The main developments and results are presented in this report.

2. AOD observation operator

2.1 Basics

Aerosol optical depth (AOD) describes the extinction of light beam traversing an atmospheric layer containing aerosol particles. Light extinction by aerosols occurs by attenuation of the incident light due to scattering and absorption. AOD (τ_{ext}) within the atmospheric layer between z_1 and z_2 is calculated as

$$\tau_{ext} = \int_{z1}^{z2} k_{ext}(\lambda, r)dz \qquad (1)$$

Here k_{ext} is the aerosol extinction coefficient at height z, z_1 and z_2 are the heights of the layer bottom and top. The extinction coefficient equals the total extinction cross-section of aerosol particles and is calculated as:

$$k_{ext}(\lambda,r) = \int_{r1}^{r2} C_{ext}(\lambda,r) \cdot N dr = \int_{r1}^{r2} \pi \cdot r^2 \cdot Q_{ext}(\lambda,r) \cdot N dr \qquad (2)$$

where r is the aerosol radius, N is the aerosol number density, r_1 and r_2 are the lower and upper radii of the particle size distribution, C_{ext} is the aerosol extinction cross-section, which can be expressed through the aerosol extinction efficiency (Q_{ext}) as $C_{ext}(\lambda,r) = \pi \cdot r^2 \cdot Q_{ext}$. Both C_{ext} and Q_{ext} are functions of the particle size and the light wavelength (λ), which are usually combined in a dimensionless size parameter $x=2\pi r/\lambda$.

Light extinction by small spherical particles can be described by Mie theory (Bohren and Huffman, 1983; Mishchenko, 2002), which key parameter is the complex refractive index of the particle relative to the surrounding air: $m= n+ik$. Complex refractive index characterises scattering (n) and absorbing (k) properties of the particle and is a specific material's property.

2.2 Revision of the AOD observation operator

Within AeroKval-2007 project, an observation operator was developed for calculating AOD based on aerosol fields produced by the EMEP chemical transport model. Two approaches were tested. The first one, a simplified AOD calculation scheme, made use of the mass concentration of aerosol components and of component specific cross-section values. The second method was based on size-resolved aerosol concentrations from the EMEP aerosol model and used the Mie scattering theory for calculating light extinction by particles.

2.2.1 Mass-based AOD approach

The calculation scheme for AOD in the mass-based approach is:

$$\tau = \sum_{k=1}^{ktop} \sum_{i=1}^{i=8} (m_{i,k} \cdot E_{ext,i})\, \Delta z_k \qquad (3)$$

Here, $m_{i,k}$ [g/m^3] is the mass concentration in the model layer k and $E_{ext,i}$ [m^2/g] is the specific cross-section of the aerosol component i, Δz_k is the depth of model vertical layer, and $k=1$ and $k=k_{top}$ are the bottom and the top layer in the model.

Compared to the previous report (Tsyro et al., 2007) some of values for cross-sections has been revised. Namely, different extinction cross-sections have been used for fine and coarse aerosols of sea salt and mineral dust (Tegen et al., 1997) in the present calculations. The values of mass specific extinction cross-section are shown in Table 1.

Table 1. Values of specific cross-sections for different aerosol components (m^2/g). (Tegen et al., 1997; Seinfeld & Pandis, 1997; Kinne et al., 2005)

	SO_4	NO_3	NH_4	OC	EC	Min. dust *)	Sea salt *)
E_{ext}	8.5	8.5	8.5	5.7	9	1.0 / 0.3	3.0 / 0.4

*) For mineral dust and sea salt, E_{ext} values are given for fine/coarse aerosols

2.2.2 AOD based on particle size distribution

Based on model calculated size distribution of particle number, AOD is derived as

$$\tau = \sum_{k=1}^{ktop} \sum_{j=1}^{4} (\pi \cdot r_j^{\,2} \cdot Q_{ext,j} \cdot N_j)\, \Delta z_k \qquad (4)$$

where r_j, N_j and $Q_{ext,j}$ are the mean radius, number concentration and extinction efficiency for the size fraction j. The extinction efficiency is calculated using the Mie code written by Michael Mishchenko, NASA GISS (Mishchenko, 2005).

As described in Tsyro et al., (2007), in order to optimise the use of computation time a pre-calculated lookup table for aerosol optical properties (e.g. extinction efficiency and extinction cross-section) is used in model runs. The table allows finding the value of Q_{ext} for the given values of particle radius and complex refractive index. The refractive index is calculated at each time step in the model, as the aerosol composition changes. As a first approximation, the effective complex refractive index (m_{eff}) for the mixture of aerosols was calculated as the sum of volume weighted complex refractive indices of all aerosol components (Tsyro et al., 2007).

Aerosol optical parameters were calculated for two types of size distribution: monodisperse within each size fraction and a superposition of (up to four) log-normal distributions. Based on published data on typical aerosol distributions, we assumed the standard deviations (σ) of 1.1, 1.4, 1.7 and 2.2 for the nucleation, Aitken, accumulation and coarse fraction respectively, and the integration size intervals were determined as $[r_g/2\sigma, r_g \cdot 2\sigma]$.

Further testing and revisions

A series of box-model tests has been performed, using the Mishchenko's Mie code, to study the dependence of particle extinction efficiency on its radius and refractive index. We have also investigated the sensitivity of extinction efficiency to the type of particle size distribution and the discretisation in the size space (size of radius increments, integration intervals). In the present work, we have confined our study of aerosol optical properties to the light wavelength of 0.55 μm. In Figure 1, calculated dependence of extinction efficiency on particle radius is shown for sulphate ($m=1.43+10^{-8}i$), organic carbon ($m=1.53+0.006i$) and elemental carbon ($m=1.95+0.79i$). Figure 1a illustrates the affect of absorption on extinction efficiency, namely, that the larger particle absorption the smoother the extinction curve (i.e. both the broad oscillations and the ripples gradually disappear) (Bohren and Huffman, 1983; Mishchenko and Travis, 2008). Namely, the function $Q_{ext}(r)$ shows a highly oscillatory behaviour for primarily scattering aerosol SO_4^{2-}, while $Q_{ext}(r)$ is much smoother for EC, which effectively absorbs the light. The implication of this is that for aerosols with radius larger than about 0.25 μm (or size

parameter x larger than 2.5-3) a finer resolution in the aerosol size is needed to accurately describe extinction efficiency of sulphate compared to elemental carbon in the case of externally mixed aerosols. The same also applies to nitrate, ammonium, organic carbon, sea salt and mineral aerosols. However, as in the EMEP model aerosols are assumed to be in an internal mixture and elemental carbon is a ubiquitous component in the mixed particles, the imaginary part of the effective refractive index is probably large enough to render a relatively smooth Q_{ext} curve.

Another effect of absorption in extinction, as described in Bohren and Huffman (1983) is that for a fixed size parameter extinction does not always increase with increasing absorption. In particular, near the absorption edge of the material increasing absorption can either decrease or increase the extinction, depending on the particle size

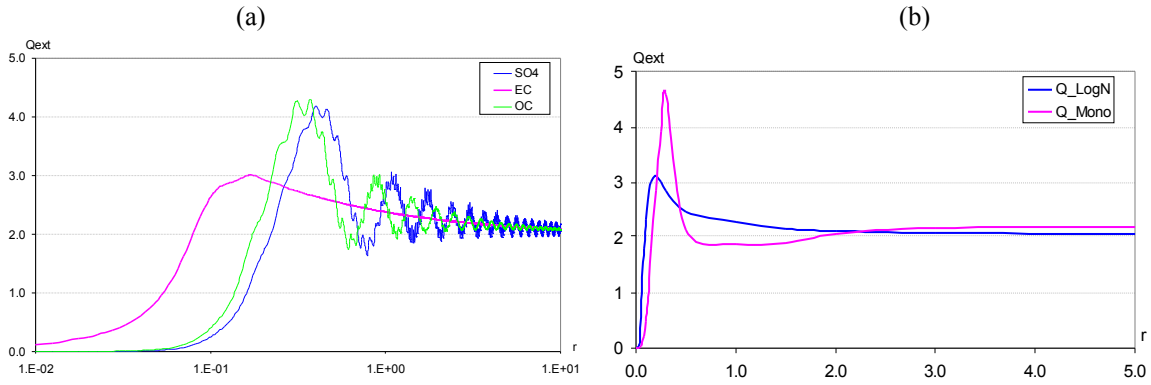

Figure 1. Extinction efficiency for the wavelength of 0.55 μm as a function of aerosol radius: a) for sulphate (refractive index $m=1.43+10^{-8}i$), elemental carbon ($m=1.95+0.79i$) and organic carbon ($m=1.53+0.006i$); b) for monodisperse and log-normally distributed sulphate aerosol.

The earlier results showed that model calculated AOD using monodisperse aerosol distribution was lower than AOD calculated assuming log-normal distribution (Tsyro et al., 2007). An example given Figure 1 shows significant differences in extinction efficiency calculated using the monodisperse and log-normal size distributions, especially for particles smaller than about 2 μm in radius. Namely, the scattering efficiency of monodisperse particles with radii smaller than 0.2 μm and larger than 0.42 μm is smaller than that of log-normally distributed particles. Thus, larger Q_{ext} for aerosol sizes within the range of 0.42-2 μm, which contribute considerably to the total scattering cross-section, is probably the main reason for the larger AOD values calculated for the log-normal aerosol distribution compared to the monodisperse particles.

The smooth behaviour of extinction efficiency as a function of particle radius for log-normally distributed aerosol is due to the effect of averaging over the size distribution. As described in e.g. Bohren and Huffman (1983) and Mishchenko et al. (2002), the features of extinction efficiency that strongly depend on particle size will be obscured, if not totally obliterated, for polydisperse aerosol. The ensemble of atmospheric particles does not exhibit the spike-like resonances because even a narrow polydispersion washes out features that strongly depend on particle size. Broadening of the size distribution (i.e. increasing the standard deviation on distribution) gradually reduces and eventually eliminates the oscillation of $Q_{ext}(r)$.

Furthermore, we have performed additional tests to study the sensitivity of Q_{ext} to the number of division points used the Mishchenko's code for calculating size-averaged optical parameters. Figure 2 shows Q_{ext} for log-normally distributed aerosol, calculated using different degree of size discretisations (N x Nk), where N is the number of integration subintervals on the size interval [Rmax, Rmin] and Nk is the number of Gaussian division points on each of the

integration subintervals. In other words, a size interval from Rmax to Rmin is resolved by totally (N x Nk) subintervals. It is seen from Figure 2 that for log-normally distributed aerosol, convergent values of extinction efficiency are already achieved at N=10 and Nk=5.

Another feature to be noted is that the slope of $Q_{ext}(r)$ curve is the steepest are for radii between 0.05 and 1.5 µm. Therefore for this radius range, the size resolution (the number of radius-increments) has been increased in the lookup table compared to the previous work in order to better describe the dependence of extinction efficiency on the particle size.

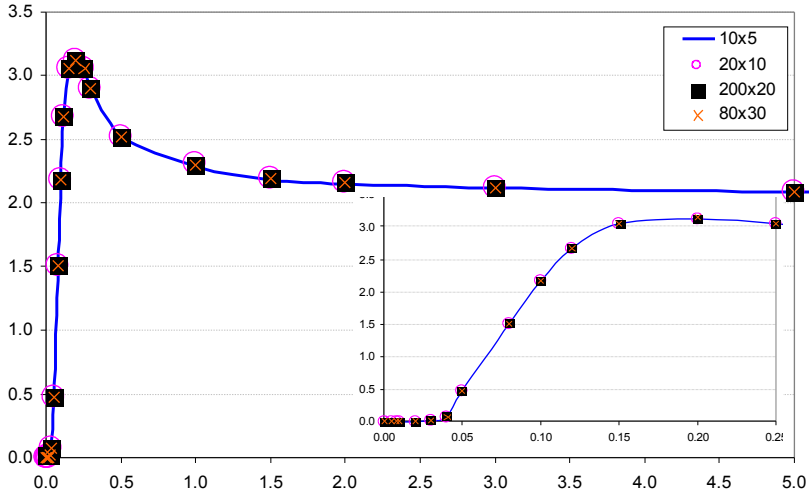

Figure 2. Extinction efficiency (Q_{ext}) calculated for log-normally distributed aerosol using different degree of size discretisations (N x Nk), where N is the number of integration subintervals on the size interval [Rmax, Rmin] and Nk is the number of Gaussian division points on each of the integration subintervals. The embedded graph is a zoom-in for the smallest particle sizes.

In summary**,** the strong dependence of scattering efficiency on aerosol size, which manifests in a highly oscillating $Q_{ext}(r)$ curve, is smoothed out when absorbing components (soot) are present in the mixed aerosols. Size averaging of $Q_{ext}(r)$ for log-normally distributed particles further smoothes it out. The tests performed with the Mie-scattering code by Mishchenko suggest that the pre-calculated lookup table provides an appropriate accuracy resolving the size dependence of extinction efficiency.

2.2.3 Effective Medium calculations

At the earlier stage of development, a volume mixing approach was used to calculate the effective refractive index of internally mixed aerosol. Recently, the method to calculate the effective refractive index has been improved by implementing the so-called Effective Medium Approximation (Michael Kahnert, *personal communications*).

For each size fraction the chemical aerosol components are assumed to be internally mixed. The effective refractive index m_{eff} of those internal mixtures is determined by use of effective medium theory (Chýlek et al., 2000). Effective Medium Approximations for m_{eff} are obtained by making assumptions on the mixing rule of different materials. When a material with refractive index m_1 is embedded into a host material with refractive index m_2 (e.g. elemental carbon coated by sulphate), the Maxwell-Garnett rule (Maxwell-Garnett, 1904) can be applied, which is given by

$$m_{eff} = \sqrt{m_2^2 \frac{m_1^{\,2}(3-2v_2) + m_2^{\,2} \cdot 2v_2}{m_1^{\,2} v_2 + m_2^{\,2}(3-v_2)}} \qquad (5)$$

where v_2 is the volume fraction of host material.

Another mixing rule which is suitable for homogeneous mixtures (e.g. sulphate and nitrate) is the Bruggeman rule (Bruggeman, 1935; Chýlek et al., 2000). In this rule the two materials are treated symmetrically, and it is written as

$$m_{eff} = \left\{ \frac{1}{4}\left[m_1^2(2-3v_2) + m_2^2(3v_2-1)\right] + \sqrt{\frac{1}{16}\left[m_1^2(2-3v_2) + m_2^2(3v_2-1)\right]^2 + \frac{1}{2}m_1^2 m_2^2} \right\}^{1/2} \qquad (6)$$

For mixtures involving more than two materials, the mixing rules can be applied iteratively. In our calculations, we apply the Bruggeman rule first for the homogeneous mixture of M=SO_4+NO_3+NH_4+OC+sea salt+ H_2O. Then, the Maxwell-Garnett rule is used for inclusions of EC and mineral dust in the mixture M. The Maxwell-Garnett and Bruggeman rules are known to yield better results for effective refractive index than simple volume-weighted mixing rules.

Based on recent results from AERONET statistics, a new, revised value of 0.0012 (instead of 10^{-8} used previously) have been used for the imaginary part of the refractive index of dust. This means a larger absorption by mineral dust in the present calculations. The real and imaginary parts of complex refractive index for the aerosol components used in the present work are provided in Table 2.

Table 2. Real (n) and imaginary (k) parts of the complex refractive index (m = n + ik) for different aerosol components used in the EMEP model

	SO_4^{2-} [1)]	NO_3^- [1)]	NH_4^+ [1)]	OC [1)]	EC [2)]	Min. dust [3)]	Sea salt [2)]	Water [4)]
n	1.43	1.43	1.43	1.53	1.95	1.5	1.56	1.333
k	10^{-8}	10^{-8}	10^{-8}	0.006	0.79	**0.0012**[*)]	0.0025	0.0

The sources are: [1)] Köpke et al. (1997), [2)] Bond and Bergstrom (2006), [3)] Sokolik and Toon (1999), [4)] Hale and Querry (1973), [*)] Michael Kahnert (*personal communications)*

2.2.4 Summary of revisions in AOD observation operator:

The major recent revisions of the AOD observation operator within the EMEP aerosol model include the following:

- Improvement of lookup table for extinction efficiency due to using a better size resolution;
- Improvement of effective refractive index calculation for mixed aerosol using the Maxwell-Garnett and Bruggeman mixing rules;
- Updating the absorption part of refractive index for mineral dust.

2.2.5 Other relevant model updates

Sea salt calculations within the EMEP model have been recently revised. The major update is an improvement of calculation of the roughness length for sea surface. Also, the parameterisation scheme for sea salt production has been refined. These revisions resulted in a larger generation of sea spray and thus the higher sea salt concentrations in model results.

3. AOD results and evaluation

In this section calculations of AOD using the revised observation operator are presented. New AOD results are compared with AOD calculated with the earlier version of the observation operator. Furthermore, we show new AOD calculations for the year of 2006 and comparison of modelled AOD with MODIS data.

3.1 AOD calculations with the EMEP model

The maps of annual mean AOD calculated with the EMEP aerosol model are presented in Figure 3. New AOD results, obtained with the revised observation operator, are displayed along with AOD calculations with the earlier version of the observation operator for 2004 (Fig. 3 upper panels). The lower panels present annual mean AOD calculated for the year of 2006 with the size distribution based and mass-based versions on the observation operator.

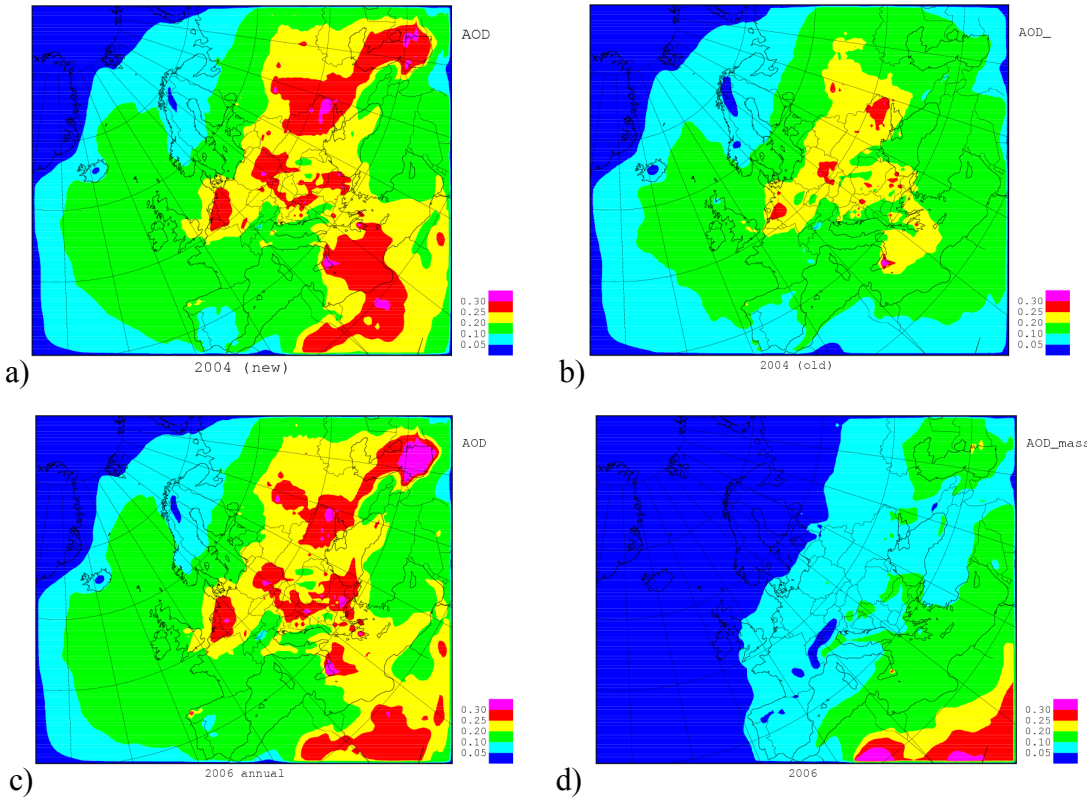

Figure 3. Model calculated annual mean AOD: for 2004 with a) revised and b) the earlier version of the observation operator; and for 2006 with the new version of observation operator c) size distribution based and d) mass-based.

In general, new AOD values calculated with the revised observation operator are higher than AOD from the earlier calculations. Several features can be further noted when looking at the AOD maps in Fig. 3. Firstly, a general pattern is obvious in the distribution of annul mean AOD in 2004 and 2006, though inter-annual AOD variations are clearly seen in several areas. Secondly, the overall AOD values produced with the observation operator based on size-distributed aerosol numbers and Mie-scattering calculations are larger than those from the operator based on aerosol mass concentrations. Inaccuracy in the mass-based AOD calculations

is partly related to the use of rather uncertain (approximate) values of specific extinction cross-sections for the aerosol components. A possible way has been considered to improve AOD calculations with the mass-based model could be to derive the specific extinction cross-sections for different aerosol types using the size-resolved model.

3.2 Comparison with MODIS retrievals

3.2.1 MODIS data

As in the previous work (Tsyro et al., 2007), MODIS aerosol data from both Terra and Aqua platforms have been used here. In addition to data from 2003 and 2004, data for 2006 (April and May) have been downloaded from the Goddard Space Flight Center (NASA) archive at http://ladsweb.nascom.nasa.gov/index.html.

Following the data precessing procedure described in Tsyro et al. (2007), aerosol products have been extracted from the downloaded Hierarchical Data Format (HDF) files, and their hourly and daily compiled data have been aggregated in the EMEP grid with 50 x 50 km^2 resolution. Here, we compare model calculated AOD with MODIS AOD retrievals at 0.55 μm wavelength, namely the MODIS product Optical_Depth_Land_And_Ocean. This product provides the data coverage for both land and ocean and is thought to have the best quality, as it only relies on primary retrieved data and has most stringent quality control.

There is an ongoing work towards further development of the observation operator in order to compare co-located model and MODIS AOD along satellite tracks (see the other report by Valdebenito and Heiberg, 2009).

3.2.2 Comparison of model calculated AOD with MODIS AOD

Model calculated AOD have been compared with AOD retrievals from MODIS data. Comparison has been made batween daily data (i.e. daily mean from the model and daily compiled from MODIS) for all grid cells within the EMEP area. Table 3 provides the comparison statistics of AOD calculated with the most recent version of observation operator and the earlier version with MODIS AOD at 0.55 μm wavelength. The comparison is made for three periods: March-April and July-August 2004, and April-May 2006. AOD obtained with the revised observation operator agrees better with MODIS AOD. In the new model results, the negative bias is considerably reduced. The correlation between calculated and MODIS AOD is now better for 2004 data, while unchanged for 2006 data.

On average, model calculated AOD is between 33 and 45% lower than MODIS retrievals. The spatial correlation coefficients vary between 0.24 and 0.36 for the periods considered. Rather low spatial correlation between AOD from the model and MODIS data could be expected due to uncertainties in both model calculations and AOD retrievals as it was discussed in the previous report (Tsyro et al., 2007). Moreover, inconsistencies between AOD calculated with the aerosol model and from MODIS data can be expected due to the principally different type of information on aerosol composition and distribution used in the AOD observation operator and in MODIS retrieval algorithm. In the model, the observation operator uses spatial distribution and chemical composition of aerosols calculated at each time step (20 minutes) to derive AOD, while the MODIS AOD retrieval algorithms rely upon prescribed aerosol types (‘aerosol models”), which are assigned pre-computed optical properties based on AERONET data. An “aerosol model” typically consists of one fine and one coarse aerosol mode and is given with rather coarse spatial (e.g. 1° x 1° grid) and temporal (monthly or seasonal) resolutions. Furthermore, the complex refractive indices may not coincide in the observation operator and MODIS retrievals.

Table 3. Bias and spatial correlation between MODIS AOD at 0.55 μm wavelength and model AOD calculated with the revised(New) and the earlier (Old) version of observation operator for the EMEP area (as in maps in Fig. 3)

Period		New	Old
March-April 2004	Bias (%)	-33	-51
	R	0.24	0.11
July-August 2004	Bias (%)	-43	-54
	R	0.36	0.26
April-May 2006	Bias (%)	-45	-51
	R	0.34	0.34

Table 4 shows the comparison statistics for AOD calculated with the revised and with the earlier version of observation operator with MODIS AOD at 0.55 μm wavelength for April-May 2006 for some model grid cells containing EMEP measurement sites. The sites with $PM_{2.5}$ (PM_{10}) observations have been selected. The comparison statistics between modelled and measured $PM_{2.5}$ (or PM_{10}) concentrations are also given in Table 4.

For most of the sites, a significantly better agreement has been achieved between calculated and MODIS AOD when using the revised observation operator. In the new results, the model underestimation of AOD is significantly smaller for all sites and the temporal correlation between calculated and MODIS AOD is higher at most of the site (except CH02, ES10, ES14, FI17).

The model underestimates AOD by between 0 and 67% for different sites compared to MODIS data. The temporal correlation between calculated and MODIS AOD is fairly good at most of the sites. It is even better than the correlation between calculated and measured $PM_{2.5}$ (or PM_{10}) for quite a few sites (shaded grey). However, it should be kept in mind that the data coverage for the considered period April-May 2006 is not necessarily the same for PM and AOD measurements. For most of the sites, fewer days with AOD data than with $PM_{2.5}$ (or PM_{10}) data were available. Therefore, the statistics for AOD and for $PM_{2.5}$ (PM_{10}) may not always be quite comparable.

3.3 Short summary

Calculation results with the EMEP aerosol model, using a revised version of the AOD observation operator, have been compared with the earlier AOD results from the first version of the observation operator. On average, the new AOD values obtained with the revised observation operator are higher than the earlier results, presented in Tsyro et al. (2007).

A better agreement has been achieved between calculated and MODIS AOD, when the revised observation operator was used. On average, model calculated AOD is between 33 and 45% lower than MODIS retrievals in different seasons in 2004 and 2006 (the model underestimation was 51-54% in the earlier tests). The spatial correlation coefficients vary between 0.24 and 0.36 for the three 2-month periods considered.

Comparison for a number of model grid cells containing EMEP measurement sites has also shown a significantly better agreement between calculated and MODIS AOD when using the revised observation operator. The model underestimation of AOD is considerably smaller and

the temporal correlation between calculated and MODIS AOD is appreciably higher for most of the sites. It is interesting to note that the temporal correlation between calculated and MODIS AOD is actually better than the correlation between calculated and measured $PM_{2.5}$ (or PM_{10}) at quite a few sites.

Table 4. Bias and correlation between MODIS AOD and model AOD calculated with the New and the Old version of observation operator for grid cells representing some EMEP sites, where statistics for $PM_{2.5}$ (PM_{10}) are also shown, for April-May 2006

	New		Old		$PM_{2.5}$ (*PM_{10}*)	
Site	Bias (%)	R	Bias (%)	R	Bias (%)	R
AT02 Illmitz	-24	0.42	-34	0.22	-30	0.51
CH02 Payerne	-35	0.52	-50	0.53	-4	0.61
CZ03 Košetice	-29	0.51	-39	0.34	-48	0.54
DE01 Westerland	-28	0.45	-40	0.29	*-15*	*0.52*
DE02 Langenbrügge	-38	0.49	-50	0.27	-43	0.46
DE44 Melpitz	-49	0.74	-57	0.46	-45	0.73
ES08 Niembro	-11	0.69	-22	0.64	17	0.64
ES10 Cabo de Creus	-62	0.09	-66	0.19	-6	0.50
ES14 Els Torms	-57	0.39	-57	0.42	-4	0.52
ES16 O Saviñao	0	0.57	10	0.52	30	0.53
FI17 Virolahti	-59	0.64	-76	0.76	52	0.43
IE31 Mace Head	-43	0.59	-48	0.68	-59	0.49
IT01 Montelibretti	-32	0.43	-37	0.38	-20	0.33
IT04 Ispra	-50	0.67	-50	0.75	-18	0.24
NO01 Birkenes	-67	0.87	-75	0.80	-14	0.51
PL05 Diabla Gora	-45	0.43	-74	0.38	*-55*	*0.47*
SE11 Vavihill	-21	0.46	-42	0.30	-27	0.29
SI08 Masun	-14	0.39	-18	0.30	-20	0.37

Grey shade - the sites where correlation between calculated and MODIS AOD is better than the correlation between calculated and measured $PM_{2.5}$ or PM_{10} (*in cursive*).

4. Further testing of AOD observation operator: Agricultural fires in spring 2006

While it is still disputable whether satellite retrievals of AOD, due to considerable uncertainties involved in the retrieval algorithms, have an appropriate quality for model evaluation, there is no doubt that the satellite observations are a powerful instrument in detecting pollution episodes, caused for example by volcano eruptions, desert storms or wildfires. Maps (images) of pollution geographical distribution based on satellite measurements can be used for testing the model ability to reproduce the pollution transport. Here, we compare AOD calculations made with the EMEP aerosol model with MODIS data for a fire pollution event in spring 2006. Modelled AOD is also compared with AOD data from sun photometers at five stations.

4.1 Fire pollution event: comparison of AOD fields from the model and MODIS

In spring 2006, large parts of Europe experienced enhanced air pollution caused by smoke from agricultural and forest fires in Eastern Europe, i.e. the Baltic States, western Russia, Belarus and Ukraine. It started with prescribed agricultural waste burning by farmers late in April, but the fire swiftly spread to the natural vegetation over large areas and went out of control. More than 300 fires per day were detected by MODIS in this area between 25 April and 6 May 2006 (Stohl et al., 2007).

The EMEP model has been used to simulate pollution episodes associated with the agricultural and forest fires in Russia and Eastern Europe in spring 2006. Monthly emissions of black and organic carbon have been taken from the Global Fire Emission Database (GFED2) at http://www.ess.uci.edu/~jranders/ (Giglio, L. et al., 2006). The monthly emissions have been distributed over the period from 15 April to 10 May based on the satellite information about the number of fires from Stohl et al. (2007).

Model calculations show that in the beginning of the considered period, the plume was transported to the north, affecting firstly Finland and northern parts of Sweden and Norway on 25 to 27 April and then the whole of Scandinavia between 28 April and 2 May. From 5 May, the main transport direction of the fire plume was westward. Between 5 and 8 May the fire plume affected central Europe. Eventually, south-eastern European countries were influenced by fire pollution in the period 5 to 12 May. The evolution of the fire plume as predicted by the EMEP model corresponds quite well with the predictions made with other models and EMEP PM measurements (Yttri and Tsyro, 2008), and with other surface in situ and remote observations (Stohl et al., 2007; Myhre et al., 2007).

Figure 4 displays a series of maps, showing the evolution of AOD filds from MODIS retrievals and from model simulations over two-week period (shown are daily maps for 27 and 29 April, 2, 6, 7 and 9 May 2006. In general, the model is doing a fairly good job reproducing the main features of AOD fields retrieved from MODIS measurements. There is quite a good resemblance between the propagation patterns of AOD associated with fires as observed by MODIS and calculated with the model. Both show the northward fire pollution transport between 27 April and 2 May. Very good agreement between model prediction and MODIS are seen for 6-7 May, when fire plume moved first to the west, reached the UK and turned north toward Iceland, where it turned east. The remaining enhanced AOD measured by MODIS 9 May is also well reproduced by the model.

As seen from Fig. 4, model calculated AOD due to fire emissions are generally lower then AOD from MODIS retrievals. This can probably be explained by uncertainties in fire emission data, both in the amount on released smoke and particularly in the emission temporal variation and injection height.

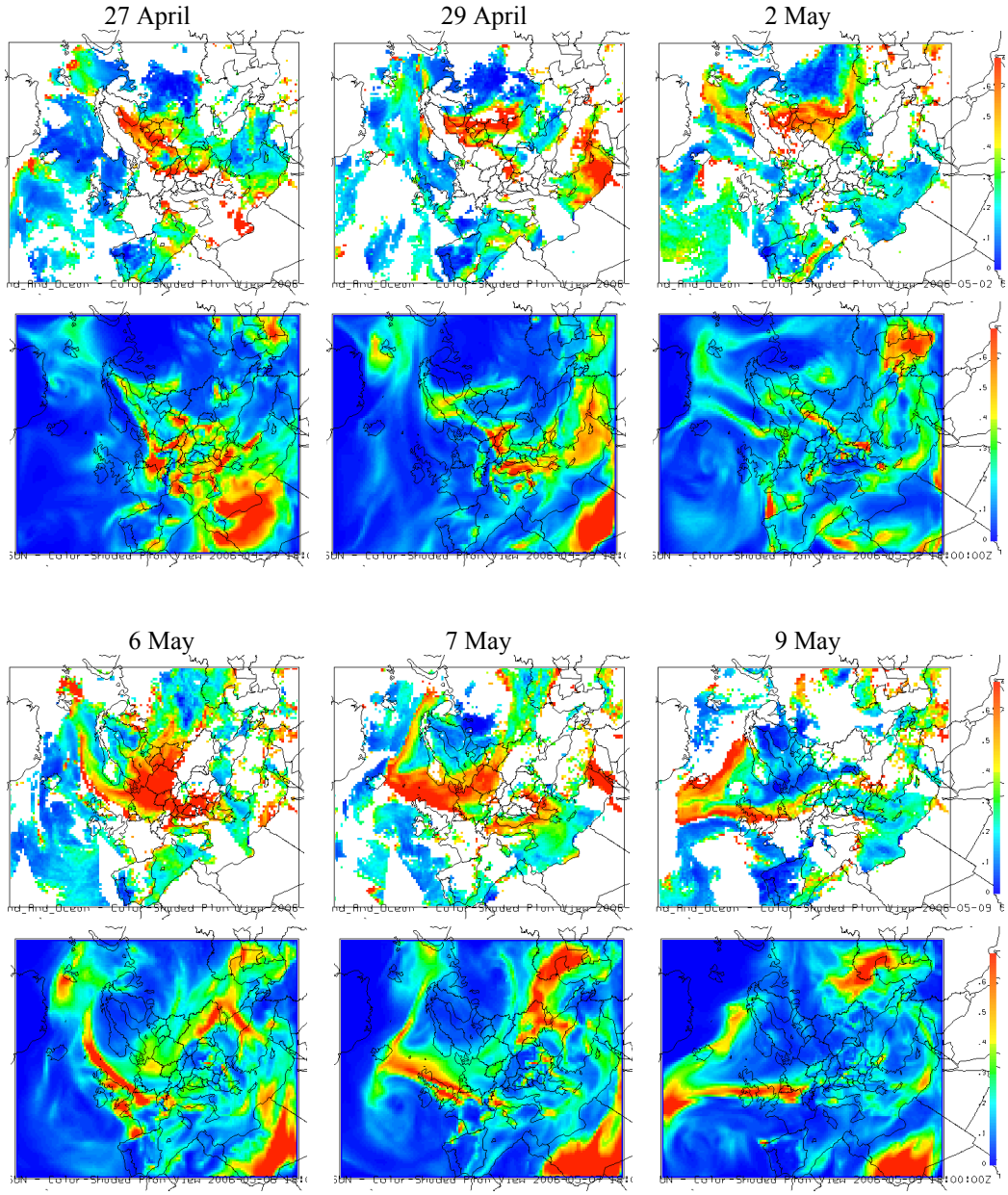

Figure 4. Daily mean model calculated AOD (bottom panels) and MODIS AOD data (upper panels) at 0.55 μm for the agricultural waste burning event in Eastern Europe in spring 2006.

4.2 Comparison of model AOD with sun photometer and MODIS data

Emission from the fires in Eastern Europe and western Russia caused several severe pollution episodes in the Northern Europe in the period between 25 April and 5 May 2006. Exceptionally high surface levels of gaseous and particulate pollutants were observed at several sites and the model was shown to manage predicting the occurrence of major PM_{10} and $PM_{2.5}$ episodes (Yttri and Tsyro, 2008).

AOD from sun photometer measurements have been made available to met.no for five sites, namely Minsk, Toravere, Sodankylä, Ny-Ålesund and Hornsund (see the map with site locations to the right) (Cathrine Lund Myhre, *personal communication*).

At sites Minsk, Toravere and Hornsund from the AERONET network (Aerosol Robotic Network), data are collected with the standard SIMEL sun photometers. At Sodankylä , where Observatory is a part of the GAW (Global Atmosphere Watch) station. AOD measurements are conducted with a Precision Filter Radiometer (PFR). At Ny-Ålesund, AOD was measured by a sky radiometer, model POM-2 (Myhre et al., 2007).

Retrieval algorithms are used to derive AOD data from satellite measurements of reflectance. As pointed out, there are uncertainties in satellite AOD data associated with uncertainties in the retrieval algorithms, which involve a number of assumptions on aerosol properties and distribution. Another potential source of inaccuracy in satellite AOD data is uncertainty in surface reflectance, especially for AOD retrievals over land. On the other hand, sun photometer AOD data are spared from this problem, as sun photometers measure the sun and sky radiances that allows a direct determining of AOD. Therefore, AOD measured with sun photometers is expected to be more accurate compared to satellite data. However, uncertainty in AOD due to data contamination by clouds is a common problem for remote sensing measurements and relies on the efficiency of screening procedures used.

In this section, we compare model calculated AOD with AOD measured by sun photometers at the five sites described above, which were affected by fires in spring 2006. In addition, modeled AOD is compared to AOD retrievals from MODIS data for the model grid cells corresponding to those sites.

Figure 5 (left column) shows the time-series of hourly AOD calculated with the model and measured by sun photometers. Quite good correlation between modelled and measured AOD, with correlation coefficient R being in a range of 0.42 to 0.87, indicates the model ability to capture pollution episodes. However, calculated AOD is significantly (by a factor 2.5-3.5 and a factor 5.5 for Hornsund)) smaller than AOD measured by sun photometers, and the underestimation is especially pronounced during the pollution episodes. This is probably because the fire emission data used in the simulations are too low.

Figure 5 (right column) shows the time-series of modelled daily AOD compared with MODIS daily compiled AOD in the same model grid cells as for sun photometers. MODIS data coverage is quite good for Minsk and Toravere site locations, but poorer for Spitsbergen and Sonankylä for the period considered. In the model results, two calculations are displayed: with fire emissions being accounted for (red curve) and disregarded (blue curve). These results show the large enhancement of AOD values due to the fire smoke in several episodes between 24 April and 6 May.

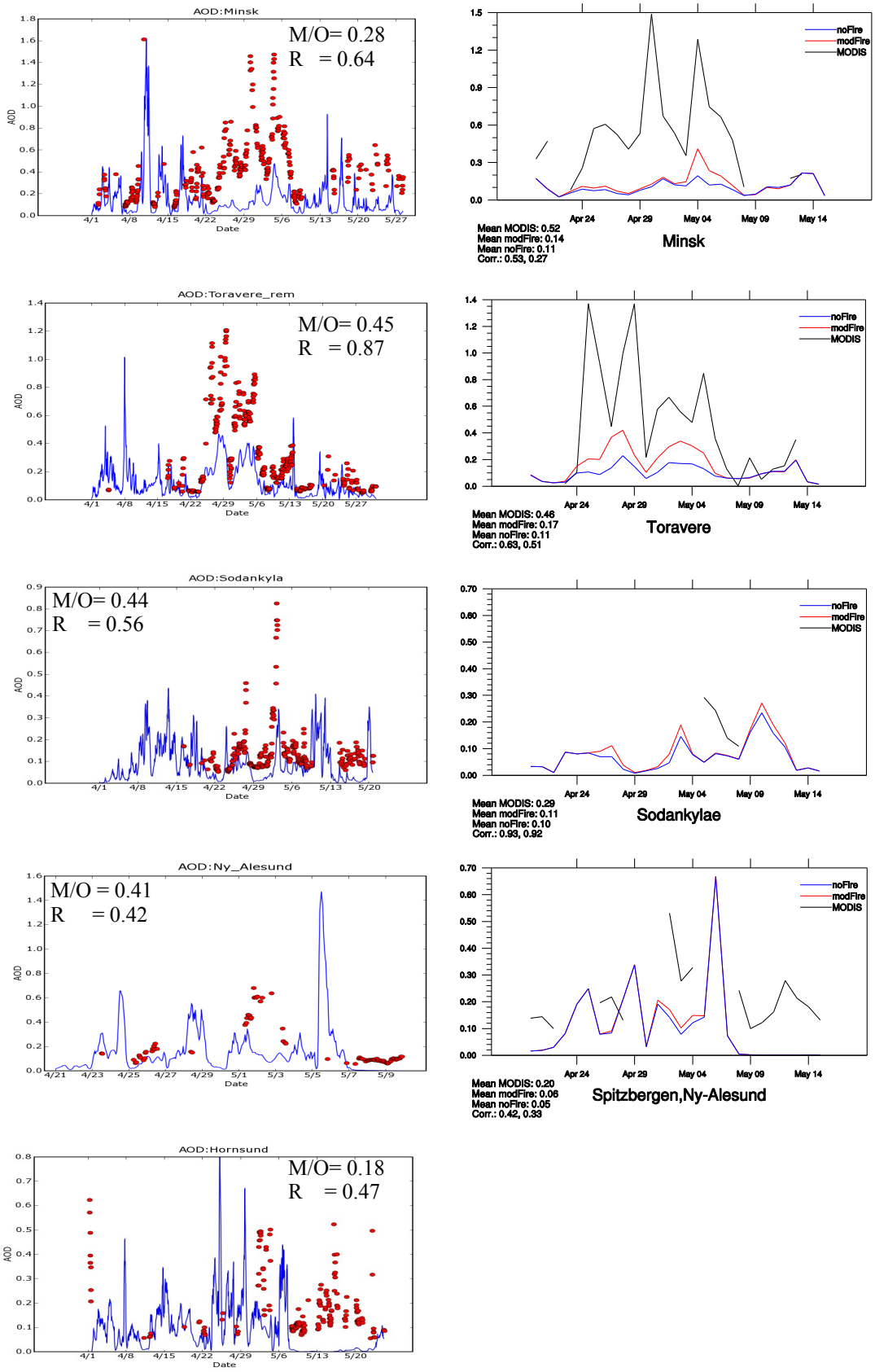

Figure 5. Time-series of: hourly modelled (blue) and sun photometer measured (red dots) AOD (left column) and daily modelled (red and blue) and MODIS (black) AOD for Minsk (BY), Toravere (EE), Sodankylä (FI), Ny Ålesund and Hornsund (NO). Here, M – model, O – observations, R – correlation coefficient.

On average, the model underestimates MODIS AOD by a factor of 2.5-3.5, which is of the same order as the model underestimation of sun photometer AOD. Also these time-series shows that the largest model underestimation of MODIS AOD occurs during the periods with enhanced AOD, i.e. when the site is affected by the fire pollution. Thus, there is a convincing indication that the emission estimates from fires are probably too low. The correlation between calculated and MODIS AOD is reasonably good, between 0.42 and 0.63, being slightly worse compared to for sun photometers.

5 Summary and outlook

In this report, the main results and findings obtained during 2008 within the AeroKval project (WP 1) are presented.

The AOD observation operator within the EMEP aerosol model, which was developed during the first year of the project and described in Tsyro et al. (2007), has been further developed and tested. Thorough testing of Mie scattering calculations with a box-model allowed us gaining more confidence in the accuracy of the lookup table for aerosol extinction efficiency, used by the AOD observation operator. The major revisions of the AOD observation operator include:

- improvement of lookup table for extinction efficiency, using a better size resolution;
- improvement of effective refractive index of mixed aerosol, implementing the Maxwell-Garnett and Bruggeman mixing rules;
- updating the absorption part of the refractive index for mineral dust.

Calculation results with the EMEP aerosol model, using the revised version of the AOD observation operator, have been presented for the years 2004 and 2006. The new AOD calculations have been compared with the AOD results from the first version of the observation operator. On average, the new AOD values produced by the revised observation operator are higher than the earlier results.

Calculated AOD has been compared with AOD retrievals from MODIS instrument on board of NASA's satellites Aqua and Terra. A better agreement, in terms of bias and correlation, has been found between calculated and MODIS AOD, when the revised observation operator was used, compared to the results from the first version of observation operator. On average, model calculated AOD is between 33 and 45% lower than MODIS retrievals in different seasons in 2004 and 2006, while the correspondent underestimation was between 51 and 54% in the earlier results. The spatial correlation coefficients vary between 0.24 and 0.36 for the periods considered.

Comparison for a number of model grid cells containing EMEP measurement sites has also shown a much better agreement between calculated and MODIS AOD when using the revised observation operator. This underestimation is considerably smaller and the temporal correlation between calculated and MODIS AOD is appreciably higher for most of the sites. The model underestimates AOD by between 0 and 67% for different sites compared to MODIS data. The temporal correlation between calculated and MODIS AOD is mostly between 0.4 and 0.7. It has been noted that for quite a few sites, the correlation between calculated and MODIS AOD is better than the correlation between calculated and measured $PM_{2.5}$ (or PM_{10}).

Further testing of the AOD observation operator has been performed using the EMEP aerosol model to simulate a pollution event due to large agricultural fires in western Russia and Eastern Europe in spring 2006. In general, the model manages quite well to reproduce the main features of AOD fields retrieved from MODIS measurements. A farly good resemblance has been found

between the propagation patterns of AOD associated with fires as observed by MODIS and calculated with the model.

Model calculated AOD has been compared with AOD measurements from sun photometers and with MODIS AOD retrievals for five sites. The model appear to be capable of predicting the occurrence of pollution episodes, as the correlation between modelled and measured AOD is between 0.42 and 0.87 for sun photometer data, and between 0.42 and 0.63 for MODIS data. However, the model underestimates both MODIS and sun-photometer measured AOD by a factor of 2.5-3.5 and the largest model underestimation of AOD is for days with enhanced AOD, i.e. when the site is affected by the fire pollution. These results are considered as an indication that the emission estimates from fires are probably too low.

Summarising the main results present here, the recent revisions of the AOD observation operator have appreciably improved the agreement between model calculations and MODIS AOD retrievals. Still, more investigation is needed to explain the cause of the model AOD underestimation compared to MODIS and sun photometer data. This would include further examination of the uncertainties in model calculated AOD, as well as gaining a better insight in satellite retrieval algorithms and critical consideration of the quality of satellite data. For validation of the model AOD results it would definitely be very valuable to involve more of sun photometer AOD measurements (and also Lidar measurements of aerosol vertical profiles). For the next year, we envisage to make a strategic review of various satellite products from different instruments and work out recommendations for future use of the satellite data for comparison with model results and for data assimilation.

Publications

Bond T. C., and R. W. Bergstrom (2006). Light Absorption by Carbonaceous Particles: An Investigative Review, Aerosol Science and Technology, 40:1, 27-67.

Bohren, C. F. and D. R. Huffman (1983). Absorption and Scattering of Light by small Particles. WILEY-VCH Verlag GmbH & Co. KGaA, Weinheim.

Bruggeman. D. A. G. (1935). Berechnung verschiedener physikalischer Konstanten von heterogenen Substanzen. 1. Dielektrizitätskonstanten und Leitfähigkeiten der Mischkörper aus isotropen Substanzen. Ann. Phys., 24:636-664.

Chýlek, P., Videen, G., Geldart, D. J. W., Steven Dobbie, J. and H. C. W. Tso. (2000) Effective medium approximations for heterogeneous particles. In M. I. Mishchenko, J. W. Hovenier, and L. D. Travis, editors, Light scattering by nonspherical particles, pp. 274-308, San Diego, 2000. Academic Press.

Giglio, L., van der Werf, G. R., Randerson, J. T., Collatz, G. J. and P. Kasibhatla (2006). Global estimation of burned area using MODIS active fire observations. Atmos. Chem. Phys., 6, 957-974.

Hale, G.M., and M.R. Querry (1973). Optical constans of water in the 200-nm to 200-mm wavelength region. Appl. Opt., 12, 555-563.

Kinne, S et al. (2006). An AeroCom initial assessment - optical properties in aerosol component modules of global models. Atmos. Chem. Phys. 6, 1815-1834.

Maxwell-Garnett, J. C. (1904). Colours in metal glasses and in metallic films. Philos. Trans. R. Soc. A, 203:385-420, 1904.

Mishchenko, M.I. and Travis, L.D. (2008) Electromagnetic scattering by particles and surfaces. http://www.giss.nasa.gov/~crmim.

Köpke, P., Hess, M., Schult, I., and E.P. Shettle (1997). Global Aerosol Dataset. Report No. 243. Max-Plank-Institut für Meteorologie. Bundesstrasse 55, D-20146, Hamburg, Germany.

Mishchenko. M. I. (2005). The program computes far-field light scattering using the Lorenz-Mie theory, and is developed by M. I. Mishchenko at NASA Goddard Institute for Space Studies, New York.

Mishchenko, M.I., Travis, L.D. and Lacis, A.A. (2002). Scattering, absorption, and emission of light by small particles. Cambridge, Cambridge University Press.

Myhre, C.L., Toledano, C., Myhre, G., Stebel, K., Yttri, K.E., Aaltonen, V., Johnsrud, M., Frioud, M., Cachorro, V., de Frutos, A., Lihavainen, H., Campbell, J.R., Chaikovsky, A.P., Shiobara, M., Welton, E.J. and Tørseth, K. (2007) Regional aerosol optical properties and radiative impact of the extreme smoke event in the European Arctic in spring 2006. Atmos. Chem. Phys., 7, 5899-5915.

Remer, L.A., D. Tanré, and Y.J. Kaufman (2006). Algorithm for remote sensing of tropospheric aerosol from MODIS: Collection 5. Product ID: MOD04/MYD04). NASA Goddard Space Flight Center, Code 913, Greenbelt, MD 20771, USA. http://modis.gsfc.nasa.gov/data/atbd/atbd_mod02.pdf

Seinfeld, J. H., S. N. Pandis (1997), "Atmospheric Chemistry and Physics; From Air Pollution to Climate Change". Wiley-Interscience, New York, USA.

Simpson, D., Fagerli, H., Jonson, J. E., Tsyro, S., Wind, P., and Tuovinen, J.-P. (2003). Transboundary Acidification, Eutrophication and Ground Level Ozone in Europe. Part I. Unified EMEP Model Description. EMEP/MSC-W Status report 1/2003 Part I. Norwegian Meteorological Institute, Oslo, Norway. http://www.emep.int.

Sokolik, I.N., and O.B Toon (1999). Incorporation of mineralogical composition into models of the radiative properties of mineral aerosol from UV to IR wavelengths. J. Geophys. Res., 104, D8, 9423-9444.

Stohl, A., Berg, T., Burkhart, J.F., Fjæraa, A.M., Forster, C., Herber, A., Hov, Ø., Lunder, C., McMillan, W.W., Oltmans, S., Shiobara, M., Simpson, D., Solberg, S., Stebel, K., Ström, J., Tørseth, K., Treffeisen, R., Virkkunen, K. and Yttri, K.E. (2007). Arctic smoke - record high air pollution levels in the European Arctic due to agricultural fires in Eastern Europe. Atmos. Chem. Phys., 7, 511-534.

Tegen, I., Hillrig, P., Chin, M., Fung, I., Jacob, D., and J. Penner (1997). Contribution of different aerosol species to the global aerosol extinction thickness: Estimates from model results. J. Geophys. Res, 102, D20, 23,895-23,915.

Tsyro, S., Heiberg, H., Klein, H., Schyberg, H., Tarrasón, L., and Jonson, J. E. (2007). First results from comparison of model calculated AOD with MODIS data. Met.no Report 11/2007. ISSN 1503-8025. Norwegian Meteorological Institute, Blindern, Norway

Tsyro, S. (2008). Regional Model for Formation, Dynamics, and Long-range Transport of Atmospheric Aerosol. Russian Meteorology and Hydrology, ISSN 1068-3739, Vol. 33, 2, 82-90.

Yttri, K. E. and S. Tsyro (2008). Agricultural Fires in spring 2006. In: Transboundary particulate matter in Europe. EMEP Status Report 4/2008.
http://www.emep.int/publ/common_publications.html